

**Optical manipulation and defect creation in a liquid crystal on a photoresponsive surface**Atefeh Habibpoumoghdam,<sup>1</sup> Lin Jiao,<sup>1</sup> Victor Reshetnyak,<sup>2</sup> Dean R. Evans,<sup>3</sup> and Alexander Lorenz<sup>1,\*</sup><sup>1</sup>*Department of Chemistry, Paderborn University, Warburger Strasse 100, 33098 Paderborn, Germany*<sup>2</sup>*Taras Shevchenko National University of Kyiv, Volodymyrska Street 64, Kyiv, 01601, Ukraine*<sup>3</sup>*Air Force Research Laboratory, Materials and Manufacturing Directorate, Wright-Patterson Air Force Base, Ohio 45433, USA*

(Received 6 January 2017; revised manuscript received 17 May 2017; published 2 August 2017)

Light-induced modulations of the refractive index and pattern formation are desirable to generate complex photonic structures via exposure to light. Here we show that local modulations of the effective refractive index and reconfigurable defects can be *locally* induced in a hybridized thin birefringent film of a nematic liquid crystal (LC) on a photoresponsive (generating photoinduced electric fields) iron doped lithium niobate surface via exposure to a focused laser beam. Samples were studied with a tailored imaging approach, which provided the ability to investigate these optically excited, field-induced responses on a microscopic level. Upon exposure with a focused laser beam, the fluent LC was expanded on the substrate's surface and localized field-induced defects were optically created. Both umbilic (central) and line defects were observed. The formation of field-induced umbilic defects was modeled in numerical simulations. In addition, line defects were experimentally studied. It was seen that line defects interconnected the centers of two central defects (field-induced defects, which were present at the upper and lower surfaces of the LC layer). In addition, line disclinations separating reverse tilt domains (caused by the inhomogeneous distribution of the photogenerated fields) were seen. These line disclinations were pinned to the central defects. By exposure with two adjacent focused laser beams two umbilic defects were created side by side and interconnected with a line defect (the line defects pinned to each umbilic defect were joined in a single defect line). An alternative technique is presented to field-induce promising photonic motives (microlenses, resonators, line defects) in a liquid crystalline, hybridized birefringent film on a microscopic scale by using a low-power laser (opposed to the high power necessary to induce optical Kerr responses in a neat LC).

DOI: [10.1103/PhysRevE.96.022701](https://doi.org/10.1103/PhysRevE.96.022701)**I. INTRODUCTION**

Photogenerated electric fields in optically responsive materials can be converted into electro-optic responses in hybridized (inorganic and organic) samples via a thin, birefringent liquid crystal (LC) film [1–4]. Iron doped lithium niobate (referred to as Fe:LN throughout this report) is a promising optically responsive candidate for the creation of photoinduced optical and electrical responses in a hybridized LC sample by using cw laser light, rather than high-energy laser pulses. Self-activated nonlinear transmission, as a result of light activated spatial filtering, and self-phase modulation have been reported [1,2] in LC test cells assembled with two Fe:LN substrates or a single Fe:LN substrate and glass plate separated by film spacers. In those studies, exposure with a focused low-power green laser beam photogenerated electric fields within the substrates, which were sufficiently large enough to excite responses in a LC (TL205) well known for low ionic contaminations. In addition, light-induced optical phase modulation was investigated in LC test cells with Fe:LN substrates, filled with the LC 5CB, and exposed to a nonfocused laser beam [3,4]. All of these previous experiments [1–4] were conducted with typical arrangements, where intensity modulations of either the excitation or the probe beam were detected with a photodetector, and could clearly reveal reversible modulations with response times (steady states) of 1–3 s. The most likely reason for light-induced electric field generation in the applied optically responsive ferroelectric materials was related to their anomalous photovoltaic responses [5], which

are capable of creating photovoltaic fields on the order of 100 kV/cm [5–7]. This effect is especially pronounced in doped ferroelectrics such as Fe:LN [6–8]. In such materials, upon exposure to visible light, a charge carrier separation along the polar crystallographic *c* axis occurs, which results in large photovoltaic fields  $E_{PV}$  at the substrate surfaces. The (reversible) experimental results with hybridized Fe:LN LC test cells in [1–4] are the product of such photogenerated fields causing electro-optical modulations within the LC layer. When the laser shutter was closed, the photogenerated electric fields decayed again, and the LC relaxed back to its initial state. This transient behavior is not unusual for photoinduced fields as it has been shown that the surface fields can be influenced by surrounding the substrates with organic dielectrics or inorganic dielectric or conductive coatings [9,10].

In this paper, optical measurements were conducted on hybrid samples comprising a Fe:LN substrate with an adjacent, well-aligned, thin layer of a LC that had relatively low optical birefringence. Point source electric fields were created in this substrate (without the need of an external power supply) via a tightly focused low-power cw laser beam with micron resolution; the resulting (optically induced) electric fields caused *localized* responses within the LC layer such as formation of topological charges or defects (i.e., single defects, connected defects), which were moved by scanning the laser beam, and even expansion of the LC film on the substrate surfaces is reported. These field-induced optical responses were investigated with polarized probe light and microscopic imaging. By use of a LC with low birefringence, well-separated birefringent stripes and characteristic Maltese cross patterns could be observed in the imaging plane, which provided highly useful experimental data that were compared to numerical simulations.

\*alexander.lorenz@uni-paderborn.de

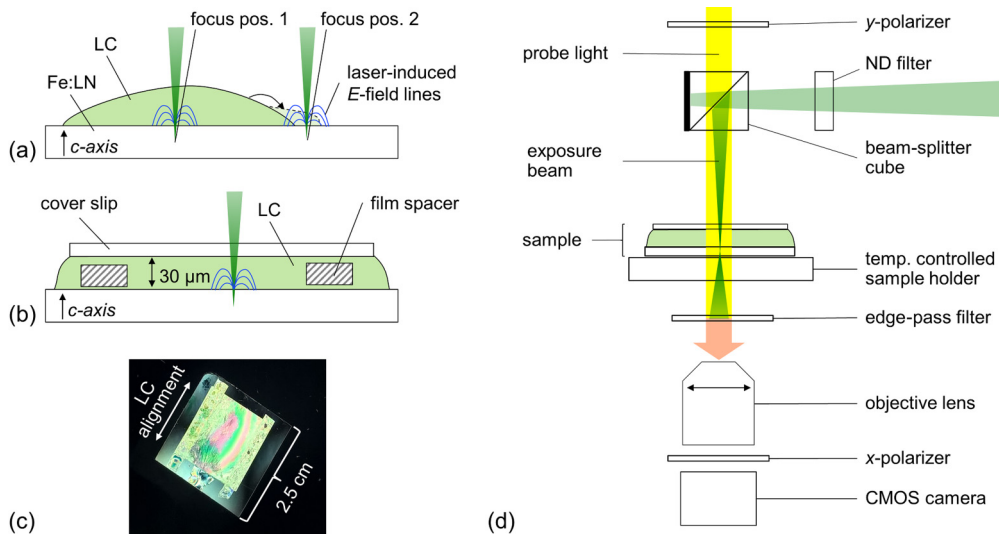


FIG. 1. (a) Schematic of the open film sample where a Fe:LN substrate was covered with an open LC film. This sample was exposed to a focused laser beam near the center of the film (focus position 1) or near the film edge (focus position 2). (b) Schematic of the sample where the LC film was confined with two film spacers and a cover slip. (c) Photograph of a confined film sample between crossed polarizers. The alignment direction (of both the Fe:LN substrate and cover slip) is indicated by a double arrow. (d) Schematic of the exposure and imaging experiment. Samples were investigated using an inverted polarized optical microscope fitted with a focused laser beam optic and rotatable polarizers. Exposure was realized with a focused green diode laser, which was coupled to the transmitted light microscopic beam path.

Furthermore, the techniques demonstrated in this paper for the photocreation of high-resolution electric fields, pixelated or patterned, result in relocatable modulations of the effective refractive index. Such controlled modulations may be useful for several applications, such as light-induced microlensing and the creation of defects, which may lead to novel possibilities to assemble microcolloids in a LC [11,12], and light moderated relocation of birefringent films in lab-on-a-chip technology. Optically created defects are well known for their high potential in both optical vortex generation [13,14] and optical trapping [12,15]. In contrast to addressing the optical Kerr effect, defects were created in hybridized samples with photogenerating substrates. The mechanism responsible for the lensing effect described in [1,2], which is known to be a result on the LC (not the substrate), is clearly explained in this paper.

## II. EXPERIMENTAL PROCEDURES

Hybrid samples comprise a Fe:LN substrate for the photogeneration of an electric field (i.e., photovoltaic effect) and a thin LC layer. Two different types of hybrids were investigated: one with an open LC film [Fig. 1(a)] and the other where a LC film was confined with film spacers and a microscopy cover slip [Fig. 1(b)]. A photograph of a confined film sample is shown [Fig. 1(c)]. Experiments were conducted with a low-birefringence nematic LC, MLC-2087, obtained from Merck KGaA. The LC was selected because of a relatively low birefringence of  $\Delta n = 0.076$ , which was desirable for observing well-separated birefringent stripe patterns in samples with local modulations of their optical axis. In a LC, the local optical axis in a small volume element can be described with a local director (a pseudovector). Since the material used has a positive sign of the dielectric anisotropy, the director (and thus the local optical axis) realigned with a tendency parallel to applied electric field lines, or in the

presented case, optically induced electric field lines. Moreover, the LC had a high clearing temperature (phase transition temperature nematic to isotropic) of  $100^\circ\text{C}$ . Both open film samples [Fig. 1(a)] and confined film samples [Fig. 1(b)] were assembled with Fe:LN substrates (Fe doping concentration 0.05 mol %, optical quality polished surfaces) obtained from Deltronic Crystal Industries,  $25 \times 25 \times 1 \text{ mm}^3$  ( $x$ ,  $y$ , and  $z$  axes, respectively). The substrates were  $z$  cut and thus their crystallographic  $c$  axis was normal to the  $xy$  plane. The  $xy$  planes of the substrates and microscopy cover slips used to assemble test cells were unidirectionally rubbed (Kimwipes, 80 times) to provide uniform alignment of the LC such that the local optical axis of the fluent material was parallel to the plane of the test cell (uniform director field) in the initial state (while not exposed to a laser beam). Open film samples [Fig. 1(a)] were obtained by depositing a small ( $0.5\text{--}1 \text{ mm}$  in diameter,  $\approx 0.5 \mu\text{l}$ ) LC droplet on the rubbed Fe:LN substrates. The droplet was spread out with a spatula to obtain an open film of LC. If so, homeotropic alignment of the LC director was induced at the air-LC interface [16]. Confined film samples were also investigated. In this case, the cells were assembled by first placing two film spacers (Mylar film) on a rubbed Fe:LN substrate and placing a microscopy cover slip (unidirectionally rubbed) on these spacers. These samples were filled with LC by placing a LC droplet near the edge of the cover slip, where the LC flowed in the gap between the substrate and the cover slip by capillary action. In these samples, a cell gap  $h$  of  $30 \mu\text{m}$  was measured with an actuating probe. These samples showed uniform (uniaxial) LC alignment.

Both types of hybrid samples were locally exposed to a tightly focused laser beam in a microscopic *imaging* setup [Fig. 1(d)], capable of investigating optical responses by use of polarized white light with micron resolution. A 4.5-mW diode laser (Thorlabs CPS 532: 532-nm wavelength, circular beam profile) was coupled to the microscope beam path of

an inverted polarized optical microscope (Olympus PMG3). The laser beam was focused in the sample plane with a lens (with focal length of 10 cm) and the laser light intensity could be adjusted with neutral density filters. The diode laser was mounted with adjusting optical stages allowing the focal position to be scanned across the sample plane to various positions with micron accuracy in order to reconfigure the light-induced field sources in the Fe:LN substrates. A beam profiler (Spiricon SP620U) was assembled in the image plane of the microscope, and a 20 $\times$  objective lens was used to image the focused laser spot; the spatial resolution of the beam profiles was calibrated with a streak plate. The laser power was monitored using a power meter (Thorlabs PM160). A Gaussian intensity distribution with a full width at half maximum of 14.3  $\mu\text{m}$  and full width of 42.5  $\mu\text{m}$  was measured. The sample, which was mounted on a temperature controlled hot stage, was illuminated with white light (probe light) and focused laser light, simultaneously. An edge-pass filter with a cut-on wavelength of 540 nm was inserted in the microscope tube to eliminate any laser light from the image plane and thereby avoid unwanted overexposure of the camera. This edge-pass filter was preferred instead of a notch filter, because it resulted in a reduced spectral range of probe light in the image plane, which was desirable to observe birefringent stripes and patterns [16] caused by director reorientations in the LC layer. The edge-pass filter was removed from the beam path to conduct adjustments of the laser beam and reinserted to investigate samples. Images were recorded with a CMOS color camera (The Imaging Source, DFK MKU120-10  $\times$  22, the camera had a 10 $\times$  zoom objective lens). Samples, where the Fe:LN substrates were replaced with (unidirectionally rubbed) glass plates, were investigated as blank tests. In these experiments, it was found that the LC did not show any light-induced responses. Moreover, these samples were investigated at temperatures between room temperature and 45  $^{\circ}\text{C}$ ; an open, single-plate hot stage was used to accommodate the sample and provide enough space for a beam splitter cube to be included in the experimental setup.

To investigate the sign [17] of topological charges induced in the LC layer of the hybrid samples, the microscope was fitted with a pair of rotatable polarizers, which were driven

by a pair of programmable stepper motors (Trinamic PD42-1141). The samples were placed between crossed polarizers, and the polarizers' rotation speeds were synchronized. This approach was preferable over rotating the sample, since it was required to expose the samples to the exposure beam during the experiment.

The dielectric anisotropy  $\Delta\epsilon$  of MLC 2087 was investigated by measuring the capacitance (HP 4284A LCR meter) of planar LC test cells (supplied by E.H.C. Co., Japan) with both homeotropic and uniform director alignment. These measurements were conducted with a sine wave signal of 1 kHz frequency and an amplitude of 0.2 V, well below the electro-optic threshold of the LC. The capacitance measured in each empty and filled LC test cell resulted in a relative dielectric constant ( $\epsilon_{\parallel} = 16.81$ ) recorded in homeotropically aligned cells and ( $\epsilon_{\perp} = 3.50$ ) recorded in uniform LC test cells, yielding a value of  $\Delta\epsilon = \epsilon_{\parallel} - \epsilon_{\perp} = 13.31$ . To obtain an estimate of the elastic constants of MLC-2087, the electro-optic threshold voltage  $V_{\text{th}}$  was measured with polarized optical microscopy in both uniform aligned LC test cells and twisted nematic LC cells by applying electric square wave signals. A threshold voltage of 1.33 V was found, which according to  $k = (V_{\text{th}}/\pi)^2 \epsilon_0 \Delta\epsilon$  [18] corresponds to an average elastic constant of  $k = 21.1$  pN. This value was used in numerical simulations (one constant approximation) of the field-induced LC realignment.

### III. RESULTS

Open film samples were exposed at two different positions [see Fig. 1(a)]. In the initial state, when the laser shutter was closed, a colorful texture [Fig. 2(a)] was observed in the open film sample at a position near the film center. The relatively broad red and green stripes, as viewed through crossed polarizers, were caused by the varying thickness of the birefringent open film. First, the sample was exposed near the center of the LC covered area [Fig. 1(a), focus position 1]. A threshold optical power of 0.20  $\mu\text{W}$  was measured (lower exposure intensities would not induce changes in the hybridized film, or only weak deformations in an area much

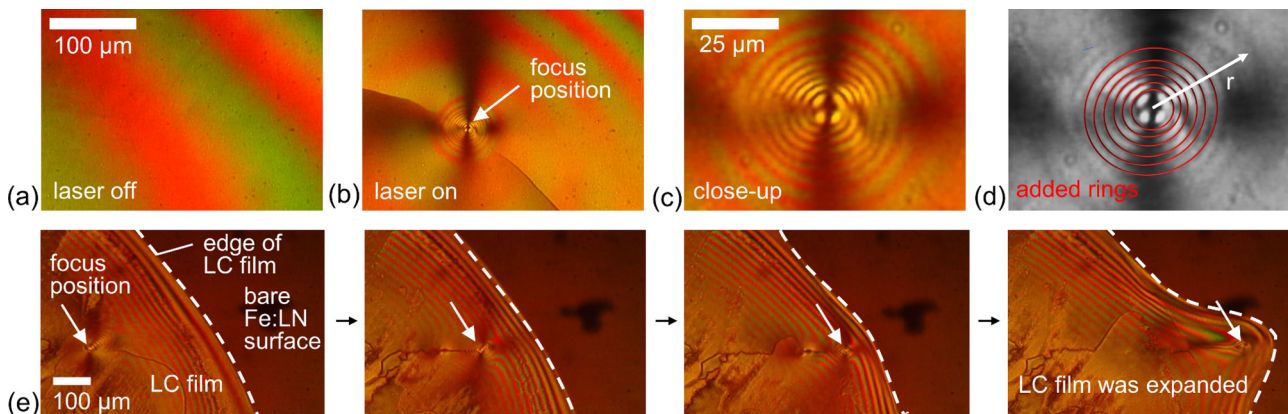


FIG. 2. Polarized optical micrographs recorded in open film samples, and associated photogenerated, field-induced defects. (a) Sample in the initial state. (b) Defect structure (central defect and defect line) observed upon exposure with a focused laser beam. (c) Closeup image of the defect center. (d) Desaturated image of the defect center. (e) Sequence of still images captured from a recorded video file showing the edge of the LC film. The edge of the LC film and the substrate surface (bare Fe:LN surface) are indicated. The focus position of the laser beam was scanned across the film edge (from left to right) within a few seconds; the film edge was thereby expanded. See Supplemental Material [25].

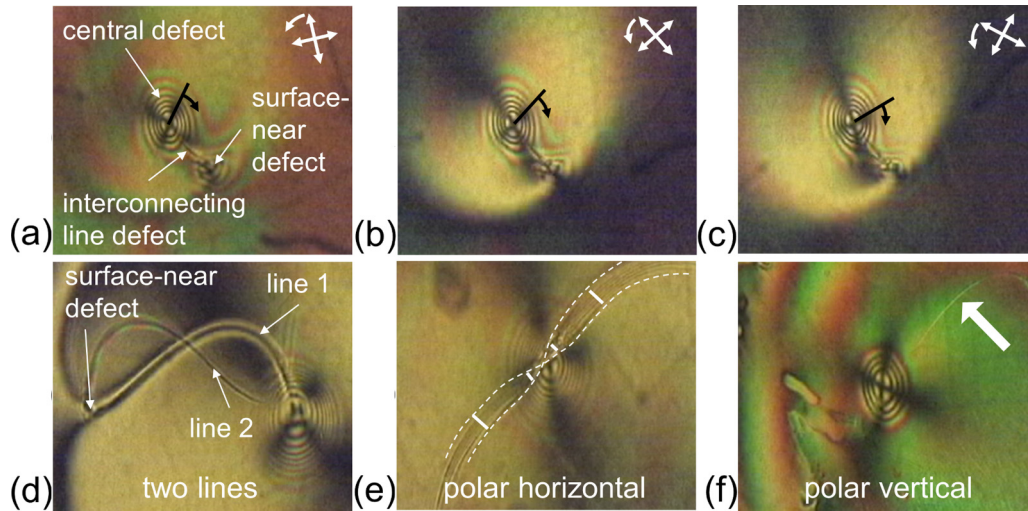


FIG. 3. Polarized optical micrographs of photogenerated field-induced defects in open film samples. (a)–(c) Series of images recorded when the crossed polarizers were rotated counterclockwise, and in turn the Maltese cross pattern was rotated clockwise: A black line is shown in one brush of the Maltese cross pattern as guide to the eye. (d) through (f) Additional images of various types of line defects observed are shown.

smaller than the beam width). Above threshold, a spotlike defect [17,19] pattern [Fig. 2(b)] was induced in the LC layer at the position of the laser focus. A closeup image of the defect pattern, which was locally induced by photogenerated fields, is also shown [Fig. 2(c)]. This closeup view was desaturated [gray-scale image, Fig. 2(d)] and, subsequently, red lines were added to show that the texture can be described by a pattern of concentric rings. Such birefringent stripes [15] are seen due to the use of polarizers and can be characteristic for electro-optic reorientations in a LC layer: The maximum possible number of stripes depends on both the film thickness  $h$  and the birefringence of the LC. From the observed pattern [Figs. 2(b)–(2d)] it can be deduced that the defect corresponds to a local variation of the optical retardation, which was caused by a realignment effect of the local optical axis inside the LC. The resultant optical retardation in each ring  $i$  can be described by  $\Delta n_{\text{eff}} h \approx i\lambda$ , where  $i$  is a small integer;  $i = 0$  can be fulfilled at the defect center if the LC is (locally) fully realigned parallel to the propagation direction of the probe light. The field-induced defects were investigated with rotated crossed polarizers. Various samples were investigated and it was found that the brushes of the Maltese cross always rotated in the inverse direction; that is, the Maltese cross texture rotated clockwise if the crossed polarizers were rotated counterclockwise. An image sequence is shown [Figs. 3(a)–(3c)]. Moreover, the texture maintained its fourfold symmetry and right angles between adjacent brushes. This behavior is characteristic [17] for a topological charge with a defect strength of -1 (a hyperbolic defect) [17]. A more detailed model of the field-induced defect is presented in Sec. IV. In addition to these features, field-induced defect lines (Fig. 3) were always visible. In the sample shown in Fig. 3(a), a second point defect (surface-near defect) was visible. This second point defect was not perfectly pinned to the laser focus position. The pair of point defects were connected by a line defect (interconnecting line defect). A pair of topological point defects (of -1 defect strength) were created on purpose [20] (by surface alignment

of the substrates) in a LC film confined with two rubbed glass substrates. This defect pair was assembled face to face and it could be shown that the pair of point defects were connected by a line defect, which expanded throughout the LC layer (an interconnecting line defect oriented perpendicular to the plane of the sample). This line defect could even be used to assemble a chain of particles, which were dispersed in the LC. The particle chain expanded from the top surface to the bottom surface of the sample and thus interconnected the substrates through the LC layer. Another example for defect lines, which occurred perpendicular to the sample plane, was microfluidic experiments [21]. It is possible that photogenerated fields caused realignment of the LC director throughout the LC layer and created a point defect pinned to the Fe:LN surface, which confined a line defect at the defect center. This line defect (interconnecting line defect) expanded through the LC layer (perpendicular to the plane of the sample). The field-induced LC realignment caused a second point defect (surface-near defect), located near the open surface of the LC film: A pair of point defects, interconnected with a line defect, was induced. It is not unusual that point defects and line defects interact. Line defects can be pinned by point defects or end in surface generated defects [22]. In addition to surface treatment and flow [20–22], also field nonhomogeneities can cause line defects, for example, in LC lenses [23,24], where centrosymmetric electric fields caused director realignments in a LC layer. As seen in Figs. 3(d)–3(f), various configurations of field-induced line defect lines were observed in the studied samples. A pair of point defects was present in the sample shown in Fig. 3(d). As in the previous example, the center of the point defect pinned to the bottom substrate (central defect pinned to the exposure position at the Fe:LN surface) was again connected to a surface-near defect by a line defect (line 1). In addition, a second defect line (line 2) appeared, which extended from the surface-near defect to the edge of the central defect. Also, two dark brushes are seen, which extend from the surface-near defect. One can speculate

whether the surface-near defect had fourfold symmetry (and was slightly deformed) or twofold symmetry [22]. Defects of both kinds were discussed [22] to pin defect lines. As in liquid crystal lenses [23,24], the nonhomogeneous field distribution (fringe fields) of the photogenerated fields led to reverse tilt domains, separated by line disclinations. Such a disclination line is a domain wall in a realigned LC, where the resulting tilt angle between the electric field and the local LC director is acute on one side of the disclination line and obtuse in the second domain (the difference of the resulting angles is often  $90^\circ$ ) [23,24]. Both polar horizontal disclination lines and polar vertical disclination lines are possible [22]. A polar horizontal disclination line is seen in Fig. 3(e). Such line defects are typically broader than a polar vertical disclination line [Fig. 3(f)] and show a birefringent striped texture. The polar horizontal disclination line [Fig. 3(e)] was aligned with director (at the line center) parallel to the sample plane near both ends and was realigned with director parallel to the photogenerated fields at the defect center (the defect line was pinned to the central defect and twisted where the photogenerated fields were perpendicular to the sample plane). The polar vertical disclination lines observed [Figs. 2(b) and 3(f)] were thinner and also led to textural changes of the LC nearby the disclination line, for example, different brightness [Fig. 2(b)]. In samples where the LC layer was confined with a cover slip (and thus the LC alignment direction was well defined), it could be deduced that the observed defect lines were always perpendicular to the rubbing direction (preferred direction of uniform LC alignment). In these samples, the evolution of defect lines could also be studied by varying the laser intensity.

The laser beam was scanned across an open film sample towards the film edge [towards focus position 2 indicated in Fig. 1(a)]. A video of the microscope field of view was recorded during this experiment and is available as Supplemental Material [25]. The laser beam was scanned stepwise and the field-induced circular defect was thereby displaced (the position of the field-induced defect was optically moved inside the LC film). In each step, the defect was first expanded (elongated) in the scanning direction, since the director reorientation was still pinned at the Fe:LN surface to the previous exposure position (until the field decayed), where the director field relaxed slowly (within 1 s) back to the initial, defect-free alignment. This relaxation was due to the decay of the optically induced fields. After relaxation, a circular defect remained, which was pinned to the new beam position. When the exposure spot reached the film edge, the LC film was expanded. A sequence of still images captured from this video file is shown in Fig. 2(e). The reason for the film expansion is the inhomogeneity of the electric field caused by the Gaussian profile of the light beam and so the photovoltaic field. The field strength is higher at the beam center. The LC was attracted to the area with the higher field strength. The physics of the LC film expansion is similar to the physics of photovoltaic tweezers [6]. The experiment shows Fe:LN substrates are promising candidates to expand and move LC films or droplets on their surfaces by scanning a laser beam with micron resolution, which should have high potential for sensing applications in microfluidic devices and lab-on-a-chip technology.

In addition to experiments with open film samples, confined film samples were also studied. In these samples, the LC

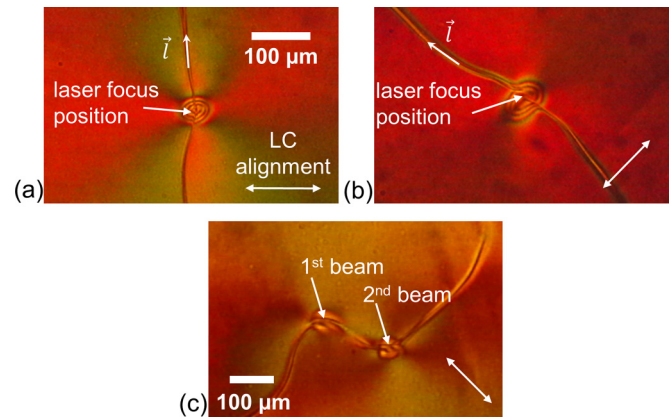


FIG. 4. Defect lines in samples with a confined LC film. The alignment direction of the LC is indicated (white double arrows) and a vector  $l$  is shown, which is parallel to the defect line. (a,b) The sample was rotated in different positions and exposed to a single focused laser beam. (c) The sample was exposed to two adjacent focused laser beams resulting in defects connected by a merged defect line.

film was confined with film spacers and defect textures can be forced by the film boundaries to be more symmetrical than in open LC films [25]. The coexistence of central and line defects could be investigated in more detail. Due to the treatment of the substrates, the optically uniaxial LC showed uniform alignment in the initial state. In the field-induced defects, fewer stripes were observed than in the open film samples because of the smaller film thickness,  $h = 30 \mu\text{m}$ . Depending on focal position and exposure intensity, birefringent ring patterns (Fig. 4) with two to five rings were observed. In addition to the central defect, polar vertical disclination lines appeared selectively. These line defects were pinned to the central defect. The sample was rotated in different positions and subsequently exposed to the focused laser beam. The recorded micrographs are shown in Fig. 4. The field-induced topological charges in the exposed samples vanished if the laser shutter was closed and the initial, defect-free alignment of the LC was recovered. The line defect was more pronounced and was spatially longer at higher exposure intensities than at lower exposure intensities. An extended experiment presented highly interesting features: a wedge cell beam splitter (with small angular splitting) was inserted in the exposure beam path to split the exposure beam into two adjacent focused spots. Two circular defects were created, one at each laser focus position. As in a confined film sample exposed to a single laser spot, a line defect appeared near (was pinned to) each of these defects. These defect lines were joined in a single line, which interconnected the central defects [Fig. 4(c)]. This interconnecting defect line may possibly have valences at both ends to interconnect more defects in experiments with more than two laser beams. This is promising, since it opens the possibility to create light-induced (i.e., electric field-induced) reconfigurable microstructures of field-induced central defects connected by line defects.

A confined film sample was exposed to various exposure intensities (Fig. 5). At low exposure intensity, a defect-free

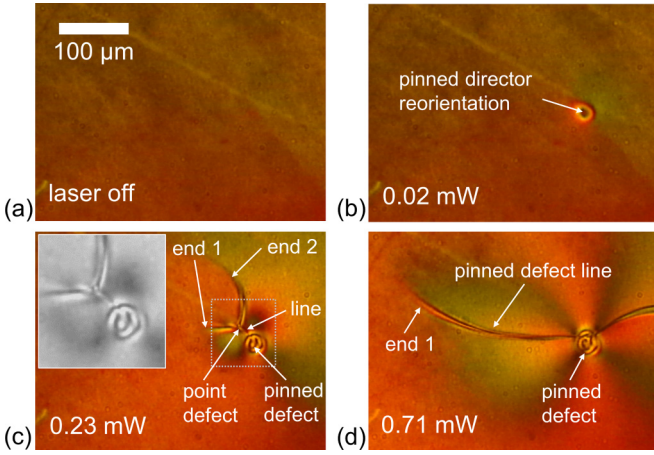


FIG. 5. Defect formation in a confined film sample observed at increasing exposure intensity. (a) Sample in the initial state. (b) Defect-free reorientation of the LC. (c) Formation of defect pair, pinned disclination line and interconnecting line defect. A magnification of the area indicated is shown as an inset. (d) Disclination line pinned to central defect.

director reorientation was observed [Fig. 5(b)]. At higher exposure intensity [Fig. 5(c)], this reorientation evolved into a pair of point defects, an interconnecting line defect, and a pinned disclination line (with two ends). The appearance of a pair of point defects was comparable to the behavior seen in Fig. 3(a) (open film sample). A section of the micrograph (showing the point defects) of the image was desaturated and is shown as an inset [Fig. 5(c)]. It is clearly seen that the pair of point defects was connected with a defect line (indicated as “line”). This defect line was 35  $\mu\text{m}$  in length (which was slightly larger than the cell gap of the sample). If the exposure intensity was further increased, this defect line was contracted and at the same time, the disclination line (pinned defect line) was expanded and was now pinned to the central defect [Fig. 5(d)]. The evolution of defects in a confined film sample showed how the central defect acted as a field-induced trap, which attracted the disclination line. Potentially, field-induced, pinned defects can be applied to manipulate rod-shaped microparticles or nanorods dispersed in a hybridized LC film (hybridized with a Fe:LN substrate).

#### IV. SIMULATIONS

The formation of field-induced defects was simulated (COMSOL MULTIPHYSICS, postprocessing in MATLAB). These simulations were challenging because a three-dimensional model was required. A hybrid aligned sample, which resembled the open film samples, turned out to be a very good approximation to numerically study the properties of the central defect. A three-dimensional model with a footprint of  $d_1 \times d_2 = 60 \times 60 \mu\text{m}^2$  was simulated with three layers (Fe:LN, LC, and air). The substrate layer was a 90- $\mu\text{m}$ -thick Fe:LN layer with relative dielectric constants of  $\epsilon_{\perp} = 85$  perpendicular and  $\epsilon_{\parallel} = 29$  parallel to the crystallographic  $c$  axis. The  $c$  axis was parallel to the  $z$  direction. The Fe:LN layer was covered with a layer of LC with a height of  $h = 30 \mu\text{m}$ . The physical properties of the LC were modeled with a

$Q$ -tensor approach [26–29], using the dielectric constants and the elastic constant measured in MLC-2087.

The three-dimensional director configuration in the LC cell was numerically modeled with a  $Q$ -tensor approach: With director-field  $n$  and scalar order parameter  $S$ , the physical properties of the LC were described with a symmetric, traceless second-rank tensor,

$$Q_{ij} = \frac{S}{2}(3n_i n_j - \delta_{ij}), \quad (1)$$

where  $\delta_{ij}$  was Kronecker’s delta ( $\delta_{ij} = 1$ , when  $i = j$ ; otherwise  $\delta_{ij} = 0$ ). The total energy per unit volume  $E$  of the LC was described by the Landau–de Gennes energy  $E_{\text{LDG}}(Q_{ij}, \nabla Q_{ij})$  and electric potential  $E_E(Q_{ij})$  [28]:

$$E = E_{\text{LDG}}(Q_{ij}, \nabla Q_{ij}) + E_E(Q_{ij}), \quad (2)$$

$$E_{\text{LDG}}(Q_{ij}, \nabla Q_{ij}) = -\frac{A}{2} Q_{ij} Q_{ij} + \frac{B}{3} Q_{ij} Q_{jk} Q_{ki} + \frac{C}{4} (Q_{ij} Q_{ij})^2 + \frac{L}{2} (\partial_k Q_{ij})(\partial_k Q_{ij}), \quad (3)$$

where coefficients  $A$ ,  $B$ ,  $C$ , and  $L$  were assumed to be constant. The first three terms represent the Landau–de Gennes potential,  $E_{\text{LDG}}^P$ , while the last term describes the elasticity of the liquid crystal ( $E_{\text{LDG}}^e$ ). With anisotropic permittivity  $\epsilon_{ij} = \bar{\epsilon} \delta_{ij} + \Delta \epsilon Q_{ij}$  of the LC and electric displacement field  $D_i = \epsilon_0 \epsilon_{ij} E_j$ , the interaction of the electric field,  $E = -\nabla V$ , was described as  $E_E = \frac{1}{2} DE$ . The electric potential  $E_E$  terms of the  $Q$ -tensor were obtained:

$$E_E = \frac{1}{2} \epsilon_0 \bar{\epsilon} \delta_{ij} (\partial_i V)(\partial_j V) + \frac{1}{3} \epsilon_0 \Delta \epsilon (\partial_j V)(\partial_k V) \frac{Q_{jk}}{S} \partial. \quad (4)$$

Minimizing the total energy of the whole volume of LC by the Euler-Lagrange method requires solving the following differential equation for the director configurations in the LC:

$$\frac{L}{2} \nabla^2 Q_{ij} + \epsilon_0 \epsilon_{ij} E_i E_j = 0, \quad (5)$$

where  $\frac{L}{2} = K$  was the effective elastic constant of the LC (one constant approximation). In the simulations, the dielectric constants and the elastic constant measured for MLC-2087 were used. LC alignment was visualized by converting the local  $Q$ -tensor data  $Q_{ij}$  to the corresponding LC director  $n$  using Eq. (1).

The initial alignment of the LC was predefined with appropriate boundary conditions (anchoring of the LC) at the upper and lower LC surfaces. The LC was covered with a 90- $\mu\text{m}$ -thick layer of air ( $\epsilon = 1$ ). A schematic of the three-layer model is shown [Fig. 6(a)]. In order to investigate the electric field-induced realignment of the LC, light-induced charge carrier separation along the crystallographic  $c$  axis of the Fe:LN substrate was assumed according to Ref. [6]. The laser beam had a Gaussian intensity profile, and therefore a centrosymmetric Gaussian distribution of charge density  $\sigma$  was used ( $\sigma = \sigma_0 e^{-(x^2+y^2)/w^2}$ ) at both the upper and lower surfaces of the Fe:LN layer (one was positively and one

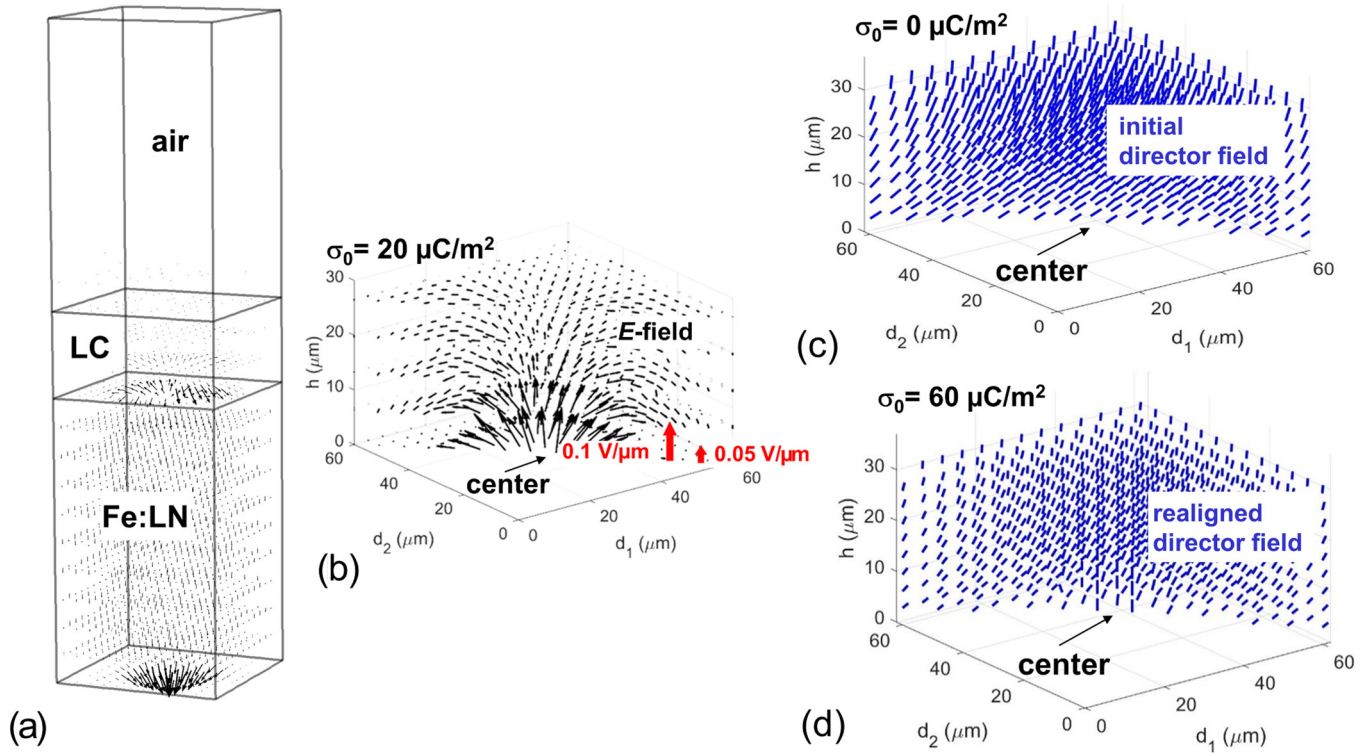


FIG. 6. Simulation of LC reorientation. (a) Schematic of the simulated three-dimensional volume. A Gaussian charge distribution was considered at the top and bottom surface of the Fe:LN layer. The obtained electric field is shown. (b) Electric-field distribution inside the LC layer. (c) Initial state: Director field with alignment parallel to  $d_1$  at the Fe:LN surface and perpendicular at the LC-air boundary. (d) Director field obtained with anchoring similar as in (c) but with charged surfaces. Please note, in (b)–(d) half of the director field is selectively shown for clarity.

was negatively charged). These Gaussian distributions were centered within the respective surfaces. The obtained electric field distribution inside the LC layer is shown [Fig. 6(b)]. The electric field obtained was highly divergent (fringe fields) and had a magnitude of  $\approx 2.2 \text{ V}/\mu\text{m}$  at the center of the charge density distribution and decayed to  $\approx 0.1 \text{ V}/\mu\text{m}$  in the area nearby the center. At the air-LC interface, homeotropic LC alignment was used [16,30]. At the lower substrates, two different alignment conditions were used. First, uniform alignment parallel to the  $d_1$  direction (rubbing direction) was simulated. This approach was useful to see if the model was capable of simulating LC realignments: A width of  $w = 10 \mu\text{m}$  and values of  $\sigma_0 = 20\text{--}60 \mu\text{C}/\text{m}^2$  were found to yield appropriate simulation results and high-enough fringe fields within the LC layer. The director field of the LC is shown in its initial state (no photoinduced electric fields) [Fig. 6(c)] and with fields present [Fig. 6(d)]. It is clearly seen that the director field was realigned by the fringe electric fields. The strictly uniform anchoring at the Fe:LN surface (parallel to the  $d_1$  direction) resulted in a director pattern with twofold symmetry. Since a defect texture with fourfold symmetry and a negative topological charge was experimentally observed, the surface anchoring at the Fe:LN surface was varied to resemble a hyperbolic defect pattern in a second simulation (Fig. 7). A negative topological charge of strength  $-1$ , as identified in the experiments, can be described [16,17,19,34] by a director field, which follows a hyperbolic pattern [Fig. 7(a)]. Placing such a director pattern through a boundary condition on the lower surface is a first order approximation, which follows

the experimental observation (of a field-induced hyperbolic defect). This approximation turned out to yield a model of the experimentally observed defect texture. As anticipated, the fourfold symmetry was maintained in the simulation result. The obtained director field in one quadrant of the simulated area is shown [Fig. 7(b)], which provides a view of the defect center and the local director orientation obtained at a charge carrier density  $\sigma_0 = 20 \mu\text{C}/\text{m}^2$ . In addition, the modulation of the transmittance of monochromatic polarized light (589 nm in wavelength, crossed polarizers) was estimated [31] by using Jones calculus. The estimated pattern [Fig. 7(c)] (full area of simulation) had fourfold symmetry and resembled the experimentally observed pattern: In addition to four dark brushes, a ring pattern can be seen. The dark areas correspond to locally, optically extinct states. Several neighboring rings are caused by a continuous variation of the optical retardation, which is low at the center of the pattern and increases continually with increasing radius. For nonpolarized light, this resembles a continuous variation of the optical path length as in a lens.

One can speculate that the field-induced defect lines, which could be observed in all samples, emerge from the center of the field-induced defect structure: An umbilic defect [30,32] in a confined LC film expands continuously over the whole LC film thickness and confines a short line defect at its center (this short line defect expands from the lower substrate surface to the upper substrate surface). Umbilic defects can be created by use of homogeneous fields (as in Ref. [30], by homogeneous magnetic fields). If so, a line defect is created and well confined

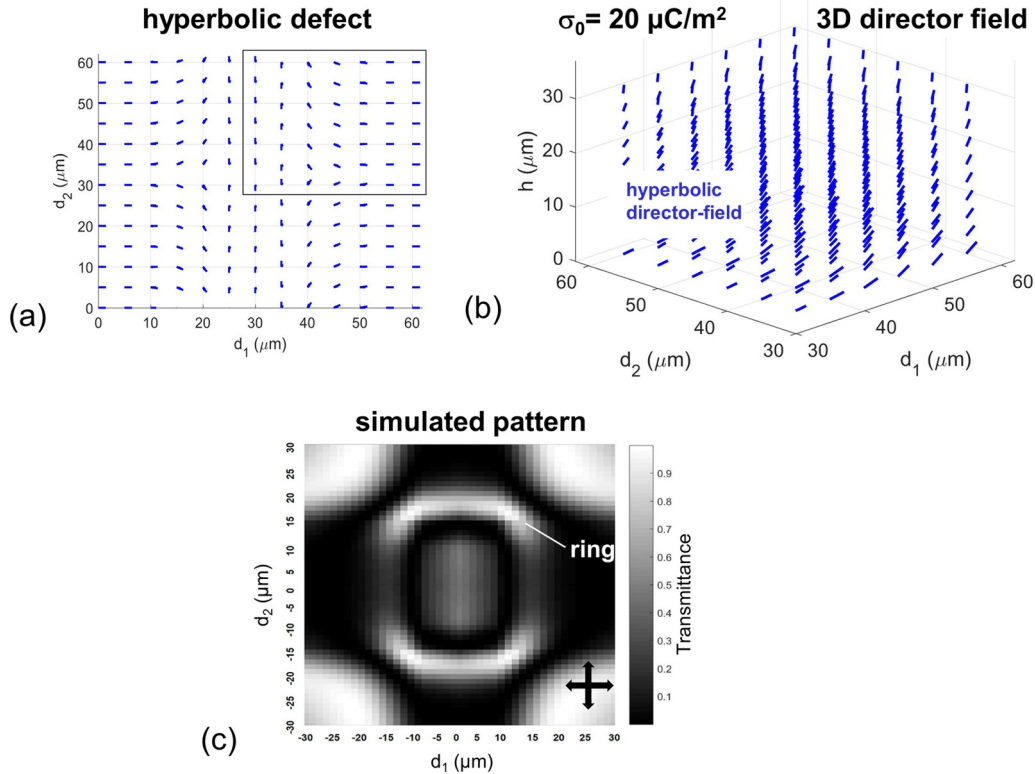


FIG. 7. (a) Director pattern in a hyperbolic defect, used as anchoring condition at the Fe:LN surface. (b) Director field in the case of hyperbolic anchoring. One quadrant is shown selectively. (c) Simulated pattern: Transmission of monochromatic light (589 nm) between crossed polarizers.

within a hyperbolic defect by two surfaces. In contrast, the observed hyperbolic defect in the investigated samples was field-induced near the Fe:LN surface with optically generated inhomogeneous electric fields. This hyperbolic defect was not confined by a second surface and the field was (along  $h$ ) both decaying and divergent. Accordingly, a line defect created at the center of the hyperbolic defect can evolve into an expanded defect line.

## V. CONCLUSIONS

In conclusion, we have investigated photoexcited field-induced responses in a hybridized LC cell (comprising liquid crystals on a field generating Fe:LN surface: no external voltage was required) using an *imaging* setup with both appropriate resolution and polarization contrast. The results obtained give evidence for field-induced reorientations in the LC layer since they reveal a Maltese cross texture, birefringent stripes, and defect lines. This was highly important for obtaining in-depth information and learning about the characteristics of light-induced director reorientations in the LC layer, which has not been possible in previous works (high-birefringence LCs, investigated with photodetectors). Polarized imaging revealed insights into the nature of specific field-induced responses such as defect formation, and was also used to reveal the sign of topological charges induced in a LC. These exciting experiments on defect formation in a LC film yield a unique method to locally manipulate a LC film with photogenerated electric fields, without the need for any externally applied voltages.

Although the samples were exposed to a focused low-power cw laser beam, both centrosymmetric defects and line defects were created via the photogenerated electric fields (i.e., they are not the result of the light itself). Defect formation occurred at the position of the exposure spot and could be easily excited at various positions and also moved within the samples. It was clearly visible that the defect lines were pinned to the central defects. Properties of the line defects were additionally studied in confined film samples. The size of the central defect was limited to 40  $\mu\text{m}$  (in diameter); the line defect could be expanded much farther (200  $\mu\text{m}$ ). The line defects were always perpendicular to the rubbing direction. Confined film samples were also manipulated effectively with two adjacent exposure beams to reveal that in such an experiment, the line defects, pinned to the central defects, were joined in a single defect line.

A first model of the director field in the central defect (open film samples) was obtained in simulations by taking into account the experimental details. In this model, the polarized optical texture of the central defect could be obtained with Jones calculus. Each point defect corresponded to a local modulation of the effective refractive index (for nonpolarized light) and thus a microlens or potentially an optical resonator can be optically induced within the hybridized LC film via optically induced electric fields. Such a microlens explains the field-induced lensing effect observed in [1,2].

Defect lines and director structures already present in a LC (intrinsically present, stimulated by alignment conditions, or by sample imperfections) can be manipulated by optical gradient forces [33] created with a focused laser beam of a

relatively low power (several mW). Now, a laser beam of even lower power (below 1 mW) was used to create and manipulate field-induced defects in a previously defect-free LC film. Field-induced defects are candidates for optical trapping and micromanipulation of colloids in a LC at very low optical power, in contrast to the high power necessary to excite optical Kerr responses in a neat LC. Thus, the presented experimental approach resulted in interesting and unexpectedly localized field-induced modulations in hybridized samples. It was found that defects can be optically induced at any position within such a film via photogenerated localized electric fields. This approach to create defects with such high resolution and manipulate the effective refractive index in a LC film has high potential to create promising field-induced photonic motives such as refractive index modulations (microlenses, resonators), and complex structures of connected defects. These can potentially be combined with colloids and de-

fects induced by colloids [11–15] to build reconfigurable, field-induced photonic structures. If the LC is doped with appropriate dyes [34], or colloids that carry quantum dot lasers, such structures may potentially even lead to optically tunable emissive photonic devices. The ability to move a fluid birefringent film across a sample surface, as demonstrated in this work, is a technique with high potential for sensing and micromanipulation applications in microfluidic devices and lab-on-a-chip technology.

#### ACKNOWLEDGMENTS

The presented research was funded by the US Air Force Office of Scientific Research (AFOSR) through the European Office of Aerospace Research and Development (EOARD) Grant No. FA9550-15-1-0426 and the German Research Council (DFG) Grants No. LO 1922/4-1 and No. GRK 1464.

- 
- [1] J. L. Carns, G. Cook, M. A. Saleh, S. V. Serak, N. V. Tabiryany, and D. R. Evans, *Opt. Lett.* **31**, 993 (2006).
- [2] J. L. Carns, G. Cook, M. A. Saleh, S. V. Serak, N. V. Tabiryany, S. A. Basun, and D. R. Evans, *Mol. Cryst. Liq. Cryst.* **453**, 83 (2006).
- [3] L. Lucchetti, K. Kushnir, A. Zaltron, and F. Simoni, *Journal of the European Optical Society: Rapid Publications* **11**, 16007 (2016).
- [4] L. Lucchetti, K. Kushnir, A. Zaltron, and F. Simoni, *Opt. Lett.* **41**, 333 (2016).
- [5] A. M. Glass, D. Von der Linde, and T. J. Negran, *Appl. Phys. Lett.* **25**, 233 (1974).
- [6] J. Villarroel *et al.*, *Opt. Express*. **19**, 24320 (2011).
- [7] M. Carrascosa, A. García-Cabañes, M. Jubera, J. B. Ramiro, and F. Agulló-López, *Appl. Phys. Rev.* **2**, 40605 (2015).
- [8] M. Esseling *et al.*, *Appl. Phys. B* **113**, 191 (2013).
- [9] P. A. Augustov and K. K. Shvarts, *Appl. Phys.* **18**, 399 (1979).
- [10] D. R. Evans, S. A. Basun, M. A. Saleh, A. S. Allen, T. P. Pottenger, G. Cook, T. J. Bunning, and S. Guha, *IEEE J. Quantum Electron.* **38**, 1661 (2002).
- [11] I. Musevic, *Science* **313**, 954 (2006).
- [12] U. Tkalec, M. Ravnik, S. Copar, S. Zumer, and I. Musevic, *Science* **333**, 62 (2011).
- [13] E. Brasselet, N. Murazawa, H. Misawa, and S. Juodkazyis, *Phys. Rev. Lett.* **103**, 103903 (2009).
- [14] E. Brasselet, *Phys. Rev. A* **82**, 063836 (2010).
- [15] L. Criante, F. Bracalente, L. Lucchetti, F. Simoni, and E. Brasselet, *Soft Matter* **9**, 5459 (2013).
- [16] O. D. Lavrentovich, *Liq. Cryst.* **24**, 117 (1998).
- [17] I. Dierking, *Textures of Liquid Crystals* (Wiley-VCH, Weinheim, 2006).
- [18] *Liquid Crystals*, edited by H. Stegemeyer (Steinkopff, Darmstadt, Germany, 1994), p. 82.
- [19] O. D. Lavrentovich and Y. A. Nastishin, *EPL* **12**, 135 (1990).
- [20] J.-B. Fleury, D. Pires, and Y. Galerne, *Phys. Rev. Lett.* **103**, 267801 (2009).
- [21] A. Sengupta, U. Tkalec, and C. Bahr, *Soft Matter* **7**, 6542 (2011).
- [22] J.-H. Lee, T. J. Atherton, D. Kang, R. G. Petschek, and C. Rosenblatt, *Phys. Rev. E* **78**, 021708 (2008).
- [23] M. Ye, B. Wang, and S. Sato, *Appl. Opt.* **43**, 6407 (2004).
- [24] C. J. Hsu and C. R. Sheu, *Opt. Express* **19**, 14999 (2011).
- [25] See Supplemental Material at <http://link.aps.org/supplemental/10.1103/PhysRevE.96.022701> for video file of an open film sample during exposure near the edge of the LC film.
- [26] G.-D. Lee, J. Anderson, and P. J. Bos, *Appl. Phys. Lett.* **81**, 3951 (2002).
- [27] H. Mori, E. C. Gartland *et al.*, *Jpn. J. Appl. Phys.* **38**, 135 (1999).
- [28] O. M. Tovkach, C. Conklin, M. C. Calderer, D. Golovaty, O. D. Lavrentovich, J. Viñals, and N. J. Walkington, *Phys. Rev. Fluids* **2**, 053302 (2017).
- [29] R. James, E. Willman *et al.*, *IEEE Trans. Electron Devices* **53**, 1575 (2006).
- [30] P. Pieranski, B. Yang, L.-J. Burtz, A. Camu, and F. Simonetti, *Liq. Cryst.* **40**, 1593 (2013).
- [31] A. Lorenz *et al.*, *Appl. Phys. Lett.* **104**, 71102 (2014).
- [32] R. B. Meyer, *Mol. Cryst. Liq. Cryst.* **16**, 355 (1972).
- [33] I. I. Smalyukh, A. N. Kuzmin, A. V. Kachynski, P. N. Prasad, and O. D. Lavrentovich, *Appl. Phys. Lett.* **86**, 21913 (2005).
- [34] D.-H. Ko *et al.*, *Appl. Phys. Lett.* **103**, 51101 (2013).